

LOW DISTORTION TITANIUM ALLOY IN LASER POWDER BED FUSION ADDITIVE MANUFACTURING

Matias Garcia-Avila¹, John Foltz¹

¹ ATI. 3875 Aeropointe Parkway, Monroe, NC 28110.

ABSTRACT

Titanium and its alloys offer superior strength at a fraction of the weight of steel or nickel-based alloys. Some α - β titanium alloys such as Ti-6Al-4V have been widely used in laser powder bed fusion additive manufacturing applications due to the historical cast-wrought data sets and the availability of this alloy in powder form, however this alloy presents challenges during the laser-based printing process of components due to the high residual stress in the material. Alternative β -rich Ti alloys such as ATI Titan 23TM can offer superior printability, lower residual stress, and higher mechanical properties than Ti-6Al-4V in additive manufacturing applications. This study covers the assessment of ATI Titan 23TM as an alternative printable Ti alloy and the resulting microstructure, mechanical properties, and residual stress of the printed material.

Citation: Garcia-Avila, Foltz, "Low Distortion Titanium Alloy in Laser Powder Bed Fusion Additive Manufacturing System," In *Proceedings of the Ground Vehicle Systems Engineering and Technology Symposium (GVSETS)*, NDIA, Novi, MI, Aug. 16-18, 2022.

1. INTRODUCTION

ATI produces titanium armor plate, sheet, and other mill products for defense vehicles. Typically, alpha-beta titanium alloys are used for these applications such as Ti-6Al-4V (Ti 64) or ATI 425[®] due to their high strength-to-weight ratio and blast and ballistic performance.

When used in armored vehicles, titanium alloys can improve efficiency from increased performance and decreased weight compared to some steel alloys. Additive manufacturing can unlock design constraints in current

components, further reducing weight and improving performance of these components.

Additive manufacturing of titanium alloys has been widely adopted in aerospace and biomedical applications and serialized production of components is well underway.

Additive manufacturing of components using titanium alloys can be challenging due to the inherent process physics and its effects on the material. In laser powder bed fusion systems for example, the directional solidification and the extremely high cooling rates experienced by the material during the melting and remelting of the layers translates into directional grain growth and high residual stresses in the material [1, 2, 3]. In

α - β titanium alloys like Ti 64, the as-printed microstructure is predominantly martensitic, which further exacerbates the residual stresses [4, 5, 6]. In addition, and due to the high β transus of Ti 64 and its fast precipitation kinetics, post-printing heat treatment options are limited to produce a final microstructure which provides balanced strength and ductility. This residual stress issue in α - β Ti alloys becomes especially important when printing large components, where large melt areas produce significant residual stress and could lead to failures during manufacturing that can render a component unprintable.

β -rich titanium alloys have the potential to avoid some of these challenges during the printing process. These alloys can improve the performance of parts made using additive manufacturing due to their slower kinetics, the suppression of martensitic transformation, and the numerous heat-treatment options to balance strength and ductility.

ATI has been developing alternative β -rich Ti alloys with slow precipitation kinetics and improved thru-section hardenability for large cross-section forgings such as landing gear and helicopter components. ATI Titan 23™ is the result of this work and achieves section hardening of up to 280mm cross-sections with superior strength, ductility, and high-cycle fatigue properties compared to Ti-10V-2Fe-3Al. For these reasons, ATI Titan 23™ was considered as a candidate for additive manufacturing trials. The details of the assessment of this alloy in a laser powder bed fusion system and results are described here.

2. MATERIALS AND PROCESSING

ATI Titan 23™ powder was manufactured at ATI Bakers Powder Operations campus in Monroe, NC. Powder was made via gas atomization using a full-scale production process and screened on-site to produce the final powder size distribution used for the

additive manufacturing trials. ATI Ti 6-4™ powder produced in the same manner is used in this study for comparison. Powder chemistry was measured using LECO combustion analysis and inductively coupled plasma mass spectroscopy. Powder size distribution of the powder was measured using laser diffraction in a Microtrac system analyzer.

Additive manufacturing printing trials were performed in a SLM 125HL LPBF machine at ATI Bakers Powder Operations campus in Monroe, NC. The process parameter development of the printing process for both ATI Titan 23™ and ATI Ti 6-4™ is beyond the scope of this paper and will not be covered here.

Hot isostatic pressing (HIP) was used to ensure full consolidation of the printed material. The HIP process was performed under argon atmosphere at 760°C temperature (below the beta transus of 815°C) and 206MPa pressure for 3 hours followed by air cool. Some material was aged post HIP at 565°C for 8 hours followed by air cool. All HIP and age heat treats were performed using NADCAP approved facilities.

Powder and microstructures of printed material were analyzed at ATI facilities using scanning electron microscopy. Micrograph preparation was performed using standard polishing practices with silicon carbide papers and finished with alumina and silica slurries. Backscatter electron imaging (BSE) and electron backscattered diffraction (EBSD) mapping was used to understand the crystallographic structure of the material in as-printed condition and after heat treatments.

X-ray diffraction (XRD) was performed at ATI on printed and heat treated material to identify phases present in the material. The XRD 2 θ scans were performed from 20° to 120° using a 40kV source at 40mA with a 2.5°/min scan speed.

For evaluation of tensile properties, cylindrical tensile specimens were printed with 13 mm diameter and 80mm length. All the specimens were HIPed and some of the specimens were also aged. The tensile specimens were machined and tested per the ASTM E8 specification [7].

Residual stresses were evaluated by measuring distortion on printed cantilever beams using previously developed techniques [8, 9].

3. RESULTS AND DISCUSSION

Chemistry results for ATI Titan 23™ powder are shown in Table 1. The powder distribution used in this study was +15/-63µm. The measured D10, D50, and D90 values of the distribution are shown in Table 1.

Table 1: Chemistry and powder size distribution results of ATI Titan 23™ Powder

V	Al	Mo	Sn	Zr	Fe	O	Ti
8.7	3.6	2.5	4.7	3.0	0.22	0.226	Bal.
Powder Size Distribution (µm)							
D10		D50		D90			
28.4		43.3		63.3			

The +15/-63µm powder morphology is shown in Figure 1. The powder produced is highly spherical with minimal satellites on the surface of the larger powder particles.

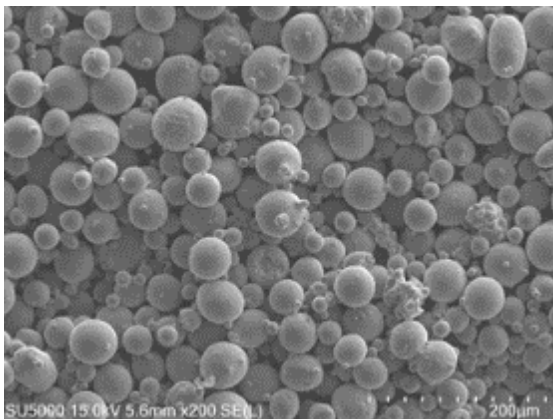


Figure 1: SEM of ATI Titan 23™ +15/-63µm powder morphology

The printed cylindrical tensile specimens are shown in Figure 2. Although no surface improvement was considered during the parameter development, the surface of the as-printed material was acceptable since the samples would be fully machined before tensile testing. Specimens were cut off the plate using a standard band saw. 6 specimens were HIPed, and after HIP was completed, 3 tensile specimens were also aged.



Figure 2: Tensile specimens printed from ATI Titan 23™ in SLM 125HL

One specimen from each condition (as-printed, as-HIPed, and HIP + age) was sectioned and polished to observe the microstructure in the build direction. Figure 3 shows a collection of SEM micrographs at two different magnifications. In the as-printed condition, ATI Titan 23™ shows no sign of martensite or α-Ti phase and is essentially only β-Ti per Figure 3. The fully retained β structure of ATI Titan 23™ alloy is a result of slow precipitation kinetics due to the alloy content; low aluminum, higher amounts of beta stabilizing elements such as vanadium and molybdenum, and in combination with the addition of Sn and Zr.

In the HIPed condition, the material precipitated primary alpha phase (dark phase) and retained large amounts of beta phase

(light grey phase) as seen in Figure 3. After aging, the retained beta phase transformed to secondary alpha phase in the form of thin laths while the primary alpha phase coarsened. Due to the alloying content, significant beta phase was retained after aging.

The EBSD results in Figure 3 show that the as-printed microstructure contained elongated beta grains in the direction of printing and no alpha crystallographic texture due to the lack of alpha phase. Upon subsequent sub-transus HIP, the beta grains recrystallize and grow forming mostly an equiaxed prior beta structure with primary alpha phase.

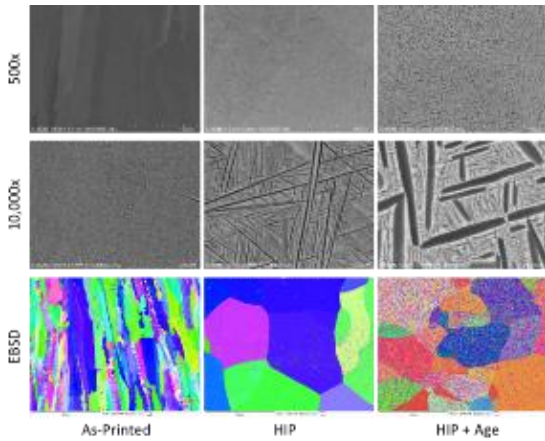


Figure 3: SEM and EBSD results on as-printed, as-HIPed (HIP), and as-HIPed plus aged (HIP + Age) ATI Titan 23™ material (build direction is vertical with respect to images)

XRD results shown in Figure 4 confirm the lack of alpha or martensite phases in the as-printed material. As observed in the microstructure, alpha phase precipitates and grows during HIP and post-HIP aging. Also shown in Figure 4 is the retained beta phase even after the aging treatment.

A total of 4 tensile specimens were tested (2 as-HIP and 2 with HIP + age). As-printed material was not tensile tested. Results for these tensile tests are shown in Figure 5 and compared with Ti 64 LPBF processed material that was annealed at 700°C for 2 hours followed by air cooling. As shown, the as-HIPed Titan 23™ shows similar tensile strength and ductility compared to Ti 64. After aging, the strength of ATI Titan 23™ increases significantly with a minimal debit to ductility. This increase in strength is due to the precipitation of secondary alpha phase as observed in the microstructure.

Figure 6 shows the results of deformation measurements due to residual stress in ATI Titan 23™ compared to Ti 64. After partial wire electric discharge machining of the cantilevers printed using a LPBF process, it was measured that ATI Titan 23™ has 75% reduction in distortion compared to Ti 64. This significant reduction in residual stress is due to the beta phase in the as printed condition of ATI Titan 23™ being more capable of accommodating residual stress

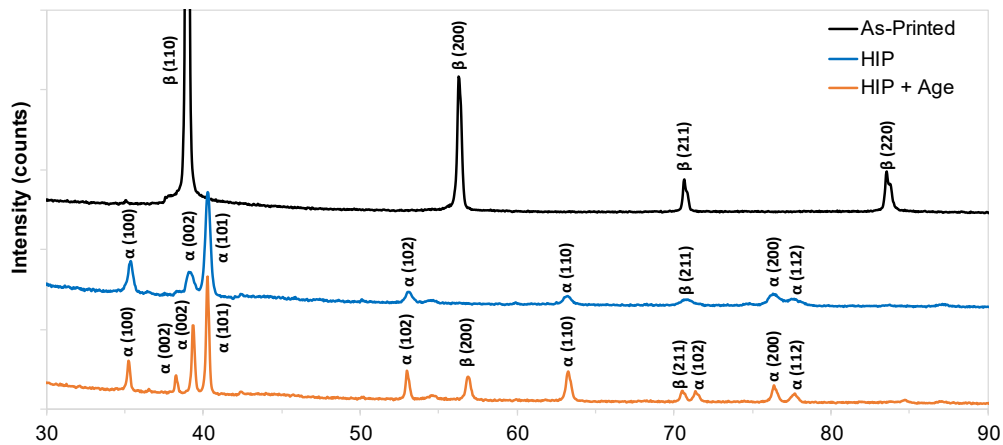


Figure 4: XRD results for material printed, HIPed, and HIPed plus aged

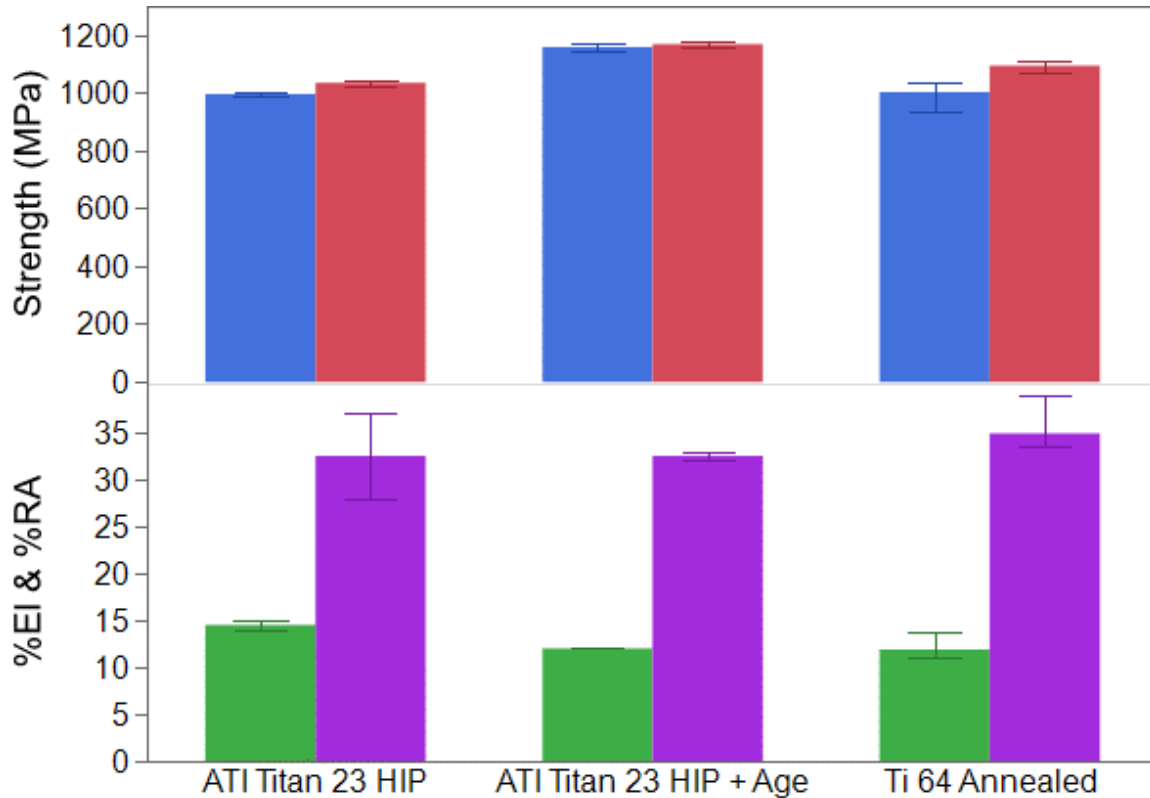


Figure 5: Tensile properties of ATI Titan 23™ in the HIP and HIP + aged conditions compared to Ti 64 annealed

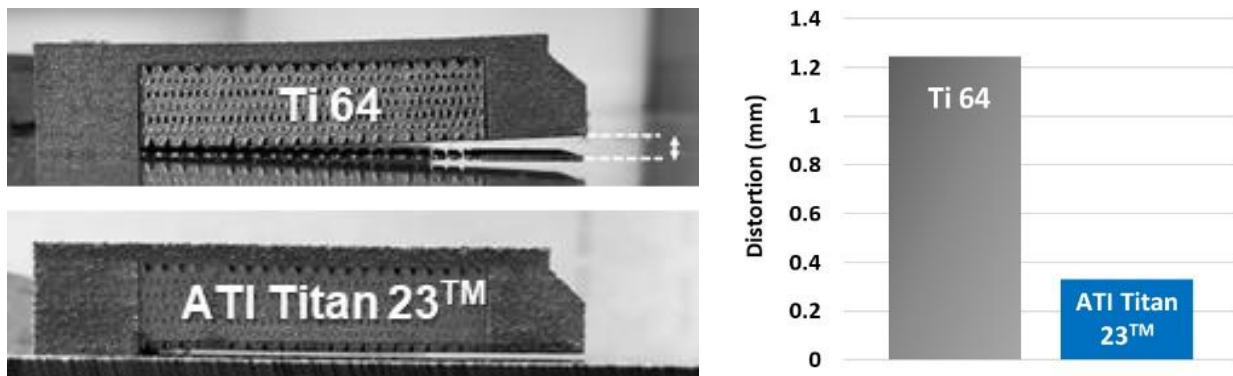


Figure 6: Deflection on Ti 64 and ATI Titan 23™ cantilevers after wire EDM cut

due to its larger number of independent slip systems and lower elastic modulus than alpha.

The drastic reduction in residual stress and distortion for LPBF-printed Titan 23™ compared to Ti 64 will enable laser-based additive manufacturing of titanium components with large cross-sections,

including applications in large defense vehicles, that may not be possible with Ti64.

4. CONCLUSION

The printability of β -rich ATI Titan 23™ alloy was evaluated in a laser powder bed fusion system. This alloy showed superior printability than Ti 64 due to the all-beta phase in the as-printed condition, avoiding

martensitic transformation during cooling, and reducing residual stresses and distortion by a factor of three compared to Ti 64. The tensile properties of ATI Titan 23TM were equivalent to Ti 64 in the as-HIPed condition, and higher in the HIP + age condition. The superior printability and higher tensile properties of ATI Titan 23TM enables the application of large printed titanium structures like those found in large defense vehicles without the issue of process-induced distortions.

5. REFERENCES

- [1] C. Li, Z.Y. Liu, X.Y. Fang, and Y.B. Guo, "Residual Stress in Metal Additive Manufacturing," *Procedia CIRP*, Vol. 71, pp. 348-353, 2018.
- [2] Erik R. Denlinger, Jarred C. Heigel, Pan Michaleris, T.A. Palmer, "Effect of inter-layer dwell time on distortion and residual stress in additive manufacturing of titanium and nickel alloys," *Journal of Materials Processing Technology*, Vol. 215, pp. 123-131, 2015.
- [3] Ó. Teixeira, F. J. G. Silva, L. P. Ferreira, and E. Atzeni, "A Review of Heat Treatments on Improving the Quality and Residual Stresses of the Ti-6Al-4V Parts Produced by Additive Manufacturing," *Metals*, vol. 10, no. 8, p. 1006, Jul. 2020.
- [4] C. Fleißner-Rieger, M. Araujo Tunes, C. Gammer, T. Jörg, T. Pfeifer, M. Musi, F. Mendez-Martin, H. Clemens, "On the existence of orthorhombic martensite in a near- α titanium base alloy used for additive manufacturing," *Journal of Alloys and Compounds*, vol. 897, 2022.
- [5] Kh. Moeinfar, F. Khodabakhshi, S.F. Kashani-bozorg, M. Mohammadi, A.P. Gerlich, "A review on metallurgical aspects of laser additive manufacturing (LAM): Stainless steels, nickel superalloys, and titanium alloys," *Journal of Materials Research and Technology*, vol. 16, pp. 1029-1068, 2022.
- [6] S. Chen, H. Gao, Y. Zhang, Q. Wu, Z. Gao, X. Zhou, "Review on residual stresses in metal additive manufacturing: formation mechanisms, parameter dependencies, prediction and control approaches," *Journal of Materials Research and Technology*, vol. 17, pp. 2950-2974, 2022.
- [7] "Standard Test Methods for Tension Testing of Metallic Materials" ASTM E8/E8M-21, in *Annual Book of ASTM Standards*, vol. 3.01. DOI: 10.1520/E0008_E0008M-21.
- [8] L. Mugwagwa, I. Yadroitsev, and S. Matope, "Effect of Process Parameters on Residual Stresses, Distortions, and Porosity in Selective Laser Melting of Maraging Steel 300," *Metals*, vol. 9, no. 10, pp. 1042, 2019.
- [9] C. Li, J. Liu, and Y.N. Guo, "Efficient Predictive Model of Cantilever Distortion in Selective Laser Melting", *Proceedings of the 27th Annual International Solid Freeform Fabrication Symposium*, Austin, TX, 2016.